Published in final edited form as:
Circulation. 2014 February 11; 129(6): 673–682. doi:10.1161/CIRCULATIONAHA.113.003026.

Bicuspid Aortic Cusp Fusion Morphology Alters Aortic 3D Outflow Patterns, Wall Shear Stress and Expression of Aortopathy

Riti Mahadevia, MD[1], **Alex J Barker, PhD**[1], **Susanne Schnell, PhD**[1], **Pegah Entezari, MD**[1], **Preeti Kansal, MD**[2], **Paul W.M. Fedak, MD**[3,4], **S Chris Malaisrie, MD**[4], **Patrick McCarthy, MD**[4], **Jeremy Collins, MD**[1], **James Carr, MD**[1], and **Michael Markl, PhD**[1,5]

[1]Department of Radiology, Feinberg School of Medicine, Northwestern University, Chicago, IL

[2]Division of Cardiology, Northwestern University, Chicago, IL

[3]Department of Cardiac Sciences, Libin Cardiovascular Institute of Alberta, University of Calgary, Canada

[4]Division of Cardiothoracic Surgery, Northwestern University, Chicago, IL

[5]Department Biomedical Engineering, McCormick School of Engineering, Northwestern University, Chicago, IL

Abstract

Background: Aortic 3D blood flow was analyzed to investigate altered ascending aorta (AAo) hemodynamics in bicuspid aortic valve (BAV) patients and its association with differences in cusp fusion patterns (right-left, RL versus right-noncoronary, RN) and expression of aortopathy.

Methods and Results: 4D flow MRI measured *in vivo* 3D blood flow in the aorta of 75 subjects: BAV patients with aortic dilatation stratified by leaflet fusion pattern (n=15 RL-BAV, mid AAo diameter=39.9±4.4mm; n=15 RN-BAV, 39.6±7.2mm); aorta size controls with tricuspid aortic valves (n=30, 41.1±4.4mm); healthy volunteers (n=15, 24.9±3.0mm). Aortopathy type (0-3), systolic flow angle, flow displacement, and regional wall shear stress (WSS) were determined for all subjects. Eccentric outflow jet patterns in BAV patients resulted in elevated regional WSS ($p<0.0125$) at the right-anterior walls for RL-BAV and right-posterior walls for RN-BAV compared to aorta size controls. Dilatation of the aortic root only (type 1) or involving the entire AAo and arch (type 3) was found in the majority of RN-BAV patients (87%) but was mostly absent for RL-BAV (87% type 2). Differences in aortopathy type between RL-BAV and RN-BAV were associated with altered flow displacement in the proximal and mid AAo for type 1 (42-81% decrease versus type 2) and distal AAo for type 3 (33-39% increase versus type 2).

Conclusions: The presence and type of BAV fusion was associated with changes in regional WSS distribution, systolic flow eccentricity, and expression of BAV aortopathy. Hemodynamic markers suggest a physiologic mechanism by which valve morphology phenotype can influence phenotypes of BAV aortopathy.

Keywords

MRI; Bicuspid Aortic Valve; Wall Shear Stress; Hemodynamics; Aortic Disease; 4D flow MRI

Correspondence: Michael Markl, PhD Department of Radiology, Northwestern University 737 N. Michigan Avenue Suite 1600, Chicago, Illinois 60611, USA Phone: 312-695-1799 Fax: 312-926-5991 michael.markl@northwestern.edu.

Conflict of Interest Disclosures:
None.

INTRODUCTION

Congenital bicuspid aortic valve (BAV) is the most common congenital cardiovascular abnormality and occurs with an incidence of 1-2% of the population [1]. This entity is associated with significant morbidity and mortality including valvular stenosis, valvular regurgitation, aortic dilation, aneurysm and dissection.[2-5] The most common distinct morphologies have been identified based on fusion patterns between the right and left coronary leaflet ("RL," frequency ~80%), the right and non-coronary leaflet ("RN," ~17%), and the less commonly left and non-coronary leaflet ("LN," ~2%) fusion patterns.[6, 7] Additionally, BAV fusion patterns have been shown to be significant as a potential predictive factor in the location and rate of development of aortic complications.[6, 8] While studies have linked genetics to the development of aortopathy in patients with BAV, the role of valve-related alterations in aortic hemodynamics and their impact on the underlying aortopathy is a reoccurring topic of debate.[9] Studies based on flow-sensitive magnetic resonance imaging (MRI), and more recently 4D flow MRI, provide evidence that the modified hemodynamic environments associated with BAV can cause altered wall shear stress (WSS) in the ascending aorta, which may trigger maladaptive vascular remodeling.[10-1314]

Studies[10, 12, 15, 16] have shown that BAV with the RL cusp fusion pattern is strongly associated with asymmetrically elevated WSS in the ascending aorta. Recent studies in individual cases[12, 16] and larger cohorts [17] have provided evidence that differences in the BAV phenotype for RL and the less common RN cusp fusion patterns can impact aortic blood flow and WSS. In addition, recent studies have shown that the type of valvular dysfunction and BAV aortopathy differ significantly between the RL- and RN-BAV phenotypes[6, 18]. Thus, the investigation of the relationship between valve fusion pattern, changes in aortic hemodynamics, and phenotype of BAV aortopathy may shed new light on the search for a mechanistic link between BAV and differences in the development of aortic pathology.

The aim of this study was therefore to evaluate the impact of different BAV cusp patterns fusion (RL and RN) on quantitative measures of aortic hemodynamics (WSS, flow angle, and flow asymmetry). Results were compared to young healthy volunteers and a dilated aorta control group matched for aortic size. We hypothesize that differences in BAV cusp morphology are associated with significant changes in aortic hemodynamics and are associated with fusion pattern specific phenotypic expression of aortopathy. Furthermore, we hypothesize that less technically involved analysis methods such as flow angle and flow displacement have the potential to provide quantitative measures of changes in regional ascending aortic hemodynamics that are associated with different types of aortic pathologies and BAV cusp fusion morphologies.

METHODS

Study Population

Patients referred for MRI to assess aortic valve morphology and function were divided into three groups: RL-BAV patients (n=15), RN-BAV patients (n=15), and patients with tricuspid aortic valves and aortic dilation (n=30) to serve as aorta size-matched controls for BAV patients. Aortic dilatation was defined as a sinus of valsalva (SOV) diameter >40mm or mid ascending aorta (MAA) diameter >40mm. Healthy young volunteers (n=15) with morphologically normal tricuspid aortic valves and no history of cardiovascular abnormalities were also included. Demographic characteristics are summarized in table 1. The study was approved by the Institutional Review Board of Northwestern University

(IRB). Informed consent was obtained from all healthy volunteers. Patients were included in accordance with an IRB protocol which permitted retrospective chart review. Informed consent was obtained from all healthy volunteers.

Magnetic Resonance Imaging

All participants underwent cardiac MRI at 1.5T or 3T (Magnetom Espree, Avanto, Skyra, or Trio, Siemens Medical Systems, Germany). All subjects underwent a standard-of-care thoracic cardiovascular MRI, including ECG gated time-resolved (CINE) cardiac MRI for the evaluation of cardiac function and valve morphology, as well as contrast enhanced MR angiography (CE-MRA) for the quantification of aortic dimensions. To assess valve morphology, breath held, ECG-gated time-resolved (2D CINE) steady state free precession (SSFP) imaging was performed in a 2D imaging plane that was carefully positioned orthogonal to the aortic root at the level of the aortic valve.

For the assessment of aortic blood flow, time-resolved 3D phase-contrast MRI with three-directional velocity encoding (4D flow MRI) was employed to measure 3D blood flow velocities with full volumetric coverage of the thoracic aorta. 4D flow MRI was acquired during free breathing using respiratory and prospective ECG gating in a sagittal oblique 3D volume of the thoracic aorta as described previously.[19] Pulse sequence parameters were as follows: flip angle = 15°, spatial resolution = 1.7-3.7mm × 1.8-2.6mm × 2.2-3.7mm, temporal resolution = 36.8-43.2ms, total acquisition time = 8-15 min depending on heart rate and navigator efficiency, velocity sensitivity = 100-300 cm/s.

Data Analysis - Valve Morphology, Aortic Diameter

Valve morphology, aortic SOV and MAA diameters, and severity of stenosis or regurgitation were determined by an experienced radiologist using standard of care imaging as described above. 2D CINE SSFP was used to assess valve morphology. CE-MRA was used to assess aortic diameter and severity of stenosis or regurgitation. Aortic dimensions were measured both at the SOV and MAA at the level of the pulmonary artery. [16, 20, 21]

Phenotypes of BAV Aortopathy

An experienced cardiac radiologist analyzed the MR angiography images for different types of aortopathy. Similar to Fazel et[22] al and Kang et al[18], different phenotypes of aortopathy were defined: type 0, normal aorta; type 1, dilated aortic root; type 2, aortic enlargement involving the tubular portion of the ascending aorta; and type 3, diffuse involvement of both the entire ascending aorta and the transverse aortic arch (see figure 1A). An aortic segment (root, ascending aorta, transverse arch) was considered dilated if a diameter >40mm was found.

Data Analysis - 4D flow MRI

Data preprocessing included noise filtering and correction for eddy currents, Maxwell terms, and velocity aliasing, as previously described by Bock et al. [23] A 3D phase contrast (PC) MR angiogram (MRA) was derived from 4D flow data and used to manually position three analysis planes in 3D visualization software (EnSight, CEI, Apex, NC, USA) at defined anatomical landmarks in the ascending aorta (figure 1): directly distal to the sinotubular junction (S1), at the midpoint between the sinotubular junction and the origin of the brachiocephalic trunk (S2), and proximal to the origin of the brachiocephalic trunk (S3). [20] Aortic 3D blood flow was visualized using 3D streamlines at peak flow systole and color coded to represent blood flow velocity (figure 2).

For each analysis plane, the aortic lumen contours were manually delineated for all time-frames using custom built software programmed in Matlab (The Mathworks, USA) to

quantify systolic valve flow angle, outflow asymmetry, and regional WSS. As shown in figure 1, valve flow angle ($\theta=\cos^{-1}[\boldsymbol{n}\bullet\boldsymbol{Q}]$) was calculated as the angle between the mean flow vector (***Q***) and a normal unit vector (***n***) orthogonal to the analysis plane. A visualization of outflow asymmetry was created by mapping the location of the upper 15% of peak systolic velocities on a segmental aortic lumen map (schematically illustrated in figure 1B). In addition and similar to the strategy reported by Sigovan et al. the 'flow displacement' distance '*d*' (in mm) from the vessel centroid to the velocity-weighted centroid was extracted as a quantitative marker to represent outflow asymmetry. [24]

Wall shear stress (WSS) was derived from the velocity data for each analysis plane by directly interpolating the local velocity derivative on the lumen contour using b-splines as described by Stalder et al.[25, 26] For each plane, regional systolic WSS was calculated at eight standardized angular segments of the aortic wall (L: left, R: right, A: anterior, P: posterior, LA: left anterior, RA: right anterior, LP: left posterior, RP: right posterior, see figure 3 for details).[16] For each analysis plane and each segment, systolic WSS was averaged over peak flow systole and 3 subsequent time points.[16] Circumferentially averaged WSS was calculated as the mean over all eight segments.

Statistical Analysis

All continuous data are presented as mean ± standard deviation. In addition, median and interquartile ranges were calculated. For each group, (healthy volunteers, aorta size matched controls, RL-BAV, RN-BAV) a Shapiro-Wilk test was used to determine if parameters were normally distributed. To compare hemodynamic parameters between the four groups, 1-way ANOVA (Gaussian distribution) or Kruskal Wallis (non-Gaussian distribution) was employed. If these tests determined that a hemodynamic parameter was significantly different between groups ($p<0.05$), multiple comparisons for all groups were performed using independent-sample t-tests (Gaussian distribution) or Mann-Whitney tests (non-Gaussian distribution). Bonferroni correction was used to adjust for multiple comparisons and differences were considered significant for $p < 0.0125$. Differences between categorical variables were assessed using Fisher's exact test. All analysis was performed using Matlab (version R2011a, The Mathworks, USA) and SPSS (version 21, IBM, USA).

RESULTS

Study Cohort

The degree of aortic valve stenosis or aortic insufficiency did not exceed "moderate" in all patients. The majority of patients had none or mild (70 of 75, 93%) stenosis or insufficiency (65 of 75, 87%). Patients with tricuspid valves were matched to aortic size for RL-BAV and RN-BAV patients (table 1). Gender distribution was similar in all groups (Fisher's exact test). Typical images for the different aortic valve morphologies are shown in figure 2. 4D flow MRI and hemodynamic analysis was successfully performed in all subjects and a complete set of flow metrics (wall shear stress, flow angle, flow displacement) was obtained in all study participants

Phenotypes of BAV Aortopathy

Among the phenotypes of aortopathy, type 2 was the most common in our BAV patients and aorta size controls (47% [28 of 60]), followed by type 1 (30% [18 of 60]) and type 3 (23% [14 of 60]). While all types 1-3 were frequently found in tricuspid aorta size controls, RL- and RN-BAV phenotypes were associated with different types of aortopathy. Noticeably, the majority (87%) of RL-BAV patients presented type 2 aortopathy while RN-BAV patients demonstrated much higher prevalence of type 1 (53%) and type 3 (34%) which were only found in two RL-BAV patients (table 1) .

3D Blood Flow Visualization

Healthy volunteers (Figure 2A) showed uniform velocity distributions with cohesive streamlines indicating flow generally parallel to the vessel walls. In contrast, highly eccentric outflow jet patterns were found in BAV patients and resulted in different flow impingement zones at the AAo wall (yellow arrows in figure 2 C and D, right anterior wall for RL-BAV, right posterior wall for RN-BAV).

Ascending Aortic Wall Shear Stress

Systolic WSS distribution in the ascending aorta showed distinct differences between valve morphologies (figure 3). Comparisons between groups revealed significant differences (Kruskal Wallis & ANOVA, range p = 1.0E-6 to p = 0.010) for all but one segment (S1, left-anterior, p=0.051). Subsequent group-wise testing showed significantly increased and highly asymmetric WSS at the level of the sinotubular junction for both BAV cohorts compared to aorta size controls. The location of significantly increased WSS was different for RL-BAV (figure 3, S1, increase in regional WSS for RA, R, RP segments) and RN-BAV (figure 3, S1, increase in regional WSS for RP, P segments) reflecting changes in localized outflow jets for different BAV cusp fusion patterns. Further downstream at the mid and distal ascending aorta (figure 3, S2 and S3), significantly increased WSS ($p<0.001$) was seen in 63-100% of segments, with RN-BAV showing the most regions of increased WSS magnitude, in agreement with the increased incidence of type 3 aortopathy in this cohort.

Flow Angle and Outflow Asymmetry

Figure 4 illustrates the magnitude and location of the top 15% of velocities at the sinotubular junction (S1) for all patient groups. Healthy volunteers showed centrally distributed peak systolic velocities (figure 4A). In contrast, peak velocities were concentrated towards the outer aortic walls in BAV patients. Consistent with differences in regionally increased WSS in figure 3, RN-BAV showed eccentric systolic outflow distributed along the right-posterior aortic wall (figure 4D) while RL-BAV demonstrated flow jets directed at the right wall in all subjects (figure 4C). Aorta size controls (figure 4B) showed less outflow asymmetry with more central locations of top 15% velocities.

Table 1 summarizes differences in flow angle and flow displacement *d* for all groups and all three analysis plane locations S1-S3. Note that flow displacements provided a better discrimination between groups. At the sinotubular junction, significantly increased flow displacement ($p < 0.0125$) was found for both BAV groups (RL-BAV: 7.6 ± 2.6mm; RN-BAV: 6.7 ± 2.6mm) compared to aorta size matched controls (3.9 ± 2.3mm) indicating the sensitivity to valve morphology induced changes in 3D aortic outflow[27].

Ascending Aorta Hemodynamics and Phenotypes of BAV Aortopathy

Figure 5 summarizes the distribution of flow angle and flow displacement *d* for BAV patients as a function of their phenotypes of BAV aortopathy. Flow displacement was most sensitive to differences in aortopathy phenotype. Note that the involvement of the distal ascending aorta (type 3) was found with increased frequency in RN-BAV while RL-BAV mostly demonstrated type 2 aortopathy. Flow displacement in patients with type 3 aortopathy (mostly RN-BAV) was predominantly increased in the mid and distal AAo (difference = 18%/39%/33% for S1/S2/S3 compared to type 2) indicating enhanced outflow asymmetry compared to patients with type 2 aortopathy phenotype (mostly RL-BAV). Moreover, type 1 aortopathy was more frequent for RN-BAV and led to reduced displacement compared to type 2 (difference = 81%/42%/16% for S1/S2/S3) which was most prominent in the proximal and mid AAo. Interestingly, circumferentially averaged peak systolic WSS did not show similar differences between aortopathy phenotypes for type

1 (maximum difference = 11%) while differences for type 3 versus type 1 were similar for all slices S1-3 (27-30%). These findings indicate the potential value of other metrics of hemodynamics such as flow displacement to identify potential mechanisms leading to the different expression of aortopathy in our BAV cohort.

DISCUSSION

The findings of this study show that the presence of BAV and type of cusp fusion pattern were accompanied by changes in systolic outflow as quantified by flow displacement, flow angles, and regional wall shear stress. In addition, we observed that altered aortic hemodynamic markers were associated with the predominant expression of aortopathy phenotype (type 2 for RL-BAV versus type 1 and 3 in RN-BAV) in our cohort.

BAV Aortopathy and Hemodynamics -Implications for BAV Management

These findings represent important new insights regarding the current recommendations of aortic diameter to influence timing and extent of surgical aortopathy management in BAV patients. The decision of how to medically manage these patients or when to operate in BAV aortopathy is difficult. Many times the degree and location of aortic dilatation is highly variable and current guidelines are supported by limited evidence. Medical management recommendations are currently based on limited evidence in Marfan patients and do not address duration of medical therapy or how to monitor for long term physiologic responses to medical therapy. When an individual is referred for surgery, the decision to resect aortic tissues in BAV aortopathy is difficult as the degree of aortic dilatation can be highly variable with respect to location on the aorta and degree of enlargement. We recently published results of a large survey of cardiac surgeons and found that operative approaches and management of BAV aortopathy is highly variable and not consistent with current guidelines[28]. Hemodynamic alterations as measured by 4D flow MRI may aid in surgical decisions with respect to the operative management of BAV aortopathy. For example, our data indicates that patients with RN cusp fusion patterns exhibit different hemodynamics and aortopathy compared to subjects with RL morphology. 4D flow MRI may thus be used to determine which regional areas of the aorta are most prone to developing complications and should therefore be resected. These initial data suggest that hemodynamic alterations and aortopathy phenotype can have variable patterns that could be important for clinical surgical management decisions.

We recognize that further studies will be needed to correlate our 4D flow MRI data with histologic morphology and clinical outcomes to further direct medical and surgical management. Novel imaging metrics such as outflow asymmetry, once validated with clinical outcomes, may be capable of shaping decisions with respect to timing and extent of aortic replacement in this diverse group of patients with BAV.

Aortic Hemodynamics - Association with BAV Fusion Pattern and Aortopathy Phenotype

Regional WSS and flow displacement revealed significant differences between patient cohorts with differing fusion patterns. Of all the metrics assessed, flow displacement was most sensitive to differences in BAV phenotype and may represent a novel and highly feasible non-invasive metric for the quantification of regional hemodynamic abnormalities in patients with bicuspid aortic valve disease.

These changes in aortic hemodynamics point to a potential explanation for the increased incidence of type 1 and type 3 aortopathy in our RN-BAV patients compared to most RL-BAV patients presenting with type 2 aortopathy. The distribution of the type of aortopathy in our cohort was similar to findings in a recent study by Kang et al[18]. We speculate that the

differences in geometry and orientation of the aortic valve in RL-BAV versus RN-BAV patients resulted in altered outflow patterns (as shown in figure 2) which can lead to changes in regional WSS and as well as flow profile asymmetry and flow displacement. In contrast, neither healthy volunteers nor aorta size matched controls showed such an obvious elevation in WSS or flow displacement at any single anatomical location across the aortic wall.

Specifically, RL-BAV patients demonstrate high velocity flow profiles (upper 15% of systolic velocities) directed towards the posterior-right-anterior wall (figure 4), as seen in-vivo and in computational models.[10, 29] For RN-BAV patients, the current study showed that the high velocity RN-BAV flow distribution was mostly contained within the right-posterior aorta and did not deviate towards the anterior wall. These findings suggest that RN-BAV flow follows a trajectory which reflects off or follows the inner curvature of the aorta to eventually impinge along the right or right posterior wall at variable heights[16]. Moreover, differences in flow displacement directly corresponded to the anatomic regions affected by different aortopathy phenotypes. Type 3 (involvement of the distal ascending aorta and transverse arch) resulted in flow displacement that was predominantly altered in the distal AAo compared to aortopathy type 2 and 1, which excluded the distal ascending aorta. In contrast, patients with type 1 (dilatation of the aortic root) exhibited highest differences in proximal AAo locations at the at the sinotubular junction and mid AAo. These findings provide evidence for a direct mechanistic link between BAV cusp fusion morphology and expression of aortopathy phenotype via a hemodynamic measure.

WSS in the younger trileaflet healthy volunteers was similar in magnitude compared to the BAV cohorts. In contrast, patients with tricuspid aortic valves and dilated aorta (aorta size controls) had significantly reduced WSS compared to the younger healthy volunteers in most segments (67%). While BAV and aortic dilatation resulted in an eccentric increase of WSS (even compared to younger healthy controls), the presence of dilatation aorta alone (with normal tricuspid valves) lead to an opposite effect on WSS, indicating the importance of cusp fusion morphology.

3D Blood Flow Visualization and Wall Shear Stress - Comparison to Previous Studies

3D visualization of in-vivo aortic 3D blood flow velocities as measured by 4D flow MRI can help to depict differences in aortic outflow between different aortic valve morphologies and provides a visual illustration of the underlying mechanisms for the development of aortopathy[10, 12, 15, 16]. It should be noted that higher velocities in the descending aorta, as seen in figure 2 are a common finding. As previously reported by Hope et al.[30], peak velocities which are initially high in the AAo show a significant slowing in the transverse aortic arch and subsequently increase when reaching the descending aorta due to a reduction in vessel diameter. The presentation and analysis of the data, however, remains semi-quantitative and is potentially subject to observer variability. Recent studies have thus shifted focus to the quantification of ascending aortic WSS, which can be directly derived from the 4D flow data, and has been implicated in the development of aortopathy[12, 15, 16]. Previous reports by Hope et al[12], Meierhofer at al[15], Bissell at al[17], and our own study[16].

The magnitude of circumferentially averaged WSS in this study (RL-BAV: 0.6 N/m^2, aorta size-matched controls: 0.3-0.4 N/m^2, healthy tricuspid volunteers: 0.6 N/m^2) were similar to those previously reported by Barker et al. (RL-BAV: 0.8±0.2 N/m^2, age-and size-matched controls: 0.4±0.2 N/m^2, healthy tricuspid volunteers: 0.4±0.1 N/m^2) and Meierhofer et al. (BAV: median 0.6 N/m^2, range 0.4-1.0 N/m^2, controls: median 0.5 N/m^2, range 0.4-0.7 N/m^2), but much lower than those by Hope et al. (RL-BAV with helical flow: 1.56 N/m^2, RL-BAV with normal flow: 1.15 N/m^2, healthy tricuspid volunteers: 0.85 N/m^2). This discrepancy is based on differences in methodology. While Hope et al. reported a WSS

maximum from all wall segments, other studies calculated systolic WSS as an average over multiple systolic time points and averaged along the wall segment.[12, 16]

Similar to previous findings, both BAV subgroups had significantly elevated WSS measured compared to aorta size matched controls.[12, 16] The finding of reduced regional WSS in aorta size controls is in excellent agreement with a recent study that reported similar findings in a cohort of n=33 patients with tricuspid aortic valve and aortic dilation compared to control groups.[29] Noticeably, extent and eccentricity of asymmetrically elevated systolic WSS in RL-BAV was similar compared to previous finding by Barker at al.[16], Hope at al[12], and Bissell et al[17]..

Alternative Metrics of Aortic Hemodynamics

Given the time-constraint and technical complexity involved with WSS quantification, many studies have explored simpler metrics as potential prognostic indicators to identify alterations in aortic hemodynamics in patients with bicuspid aortic valves.[24, 31, 32] For example, restricted “cusp opening angle” was recently shown to differentiate BAV patients from healthy volunteers (BAV fused leaflet: 62° ± 5°, healthy tricuspid volunteers: 75° ± 3°, $p<0.001$) and was strongly correlated with ascending aortic diameters and growth rate ($p<0.001$). [31] “Systolic left ventricle outflow jet angle,” or the angle between the experimental flow vector and theoretical axis of left ventricular outflow, was another such measure that differentiated BAV patients from healthy tricuspid volunteers (BAV: 17.54°± 0.87°, healthy volunteers: 10.01° ± 1.29°, $p<0.01$) and correlated with aortic dilation in BAV patients ($p<0.05$).[32] To avoid more than one vector calculation and co-registration of two datasets, Sigovan et al. modified den Reijer et al.’s approach to develop two metrics: flow angle and flow displacement.[24, 32] Similar to our findings, Sigovan et al. found that flow displacement was the most sensitive marker and was significantly elevated in patients with marked eccentric flow compared to the mild eccentric cohort (0.18±0.03 versus 0.12±0.05, $p<0.04$).

Study Limitations

A limitation of this study is the lack of longitudinal outcomes which underlines the feasibility character of our study. Future studies would benefit from a greater number of patients within each cohort and the inclusion of additional congenital valve abnormality phenotypes, such as those with equal-sized valve (true BAV without raphe) or unicuspid valves [7]. While aorta size controls were carefully selected to match aortic dilatation on the BAV cohort, differences in age remain. It should be noted that the results presented in this manuscript have not been adjusted for age or other differences in patient characteristics. However, since aortic dilatation occurs at a much younger age in BAV patients, it was not possible to match the BAV and control cohorts for age and covariate adjustment may thus not appropriately reflect age related effects. Further studies are warranted to systematically investigate the combined influence of age and type of valve abnormality on metrics of aortic hemodynamics. Another limitation is that healthy volunteers were not age-matched to the other three cohorts. This may be addressed by recruiting older participants to serve as healthy volunteers.

WSS quantification is a time-consuming and technically complex analysis. Future investigation and utilization of measures such as outflow asymmetry and flow displacement may offer a novel index that is easier to obtain and has the potential to be automated. Additional studies are needed to systematically investigate the relationships between different measures of altered aortic blood flow and their association with the development of aortopathy. Most importantly, longitudinal studies are required to link altered

hemodynamics and progression of aortic disease with medical management and surgical resection strategies.

Conclusion

Our study shows that the presence and type of BAV fusion was associated with changes in regional WSS distribution, systolic outflow asymmetry, and expression of BAV aortopathy. Of the parameters measured, flow displacement was most sensitive to differences in BAV phenotype and may represent a new and easily accessible metric for the quantification of hemodynamic abnormalities in aortic valve disease. Future longitudinal studies are warranted to evaluate the impact of BAV valve morphology and the associated hemodynamic alterations in determining risk for aortopathy development and progression.

Supplementary Material

Refer to Web version on PubMed Central for supplementary material.

Acknowledgments

Funding Sources: This study was supported by NIH NHLBI grant R01HL115828; NUCATS Institute NIH grant UL1RR025741, and the Northwestern Memorial Foundation Dixon Translational Research Grants Initiative; American Heart Association Scientist Development Grant 13SDG14360004. Additional support by the Northwestern's Bicuspid Aortic Valve Program at the Bluhm Cardiovascular Institute.

References

1. Fedak PWM, Verma S, David TE, Leask RL, Weisel RD, Butany J. Clinical and pathophysiological implications of a bicuspid aortic valve. Circulation. 2002; 106:900–904. [PubMed: 12186790]
2. Michelena HI, Khanna AD, Mahoney D, Margaryan E, Topilsky Y, Suri RM, Eidem B, Edwards WD, Sundt TM 3rd, Enriquez-Sarano M. Incidence of aortic complications in patients with bicuspid aortic valves. JAMA. 2011; 306:1104–1112. [PubMed: 21917581]
3. Mordi I, Tzemos N. Bicuspid aortic valve disease: A comprehensive review. Cardiol Res Pract. 2012; 2012:7.
4. Rudolph, AM. Congenital diseases of the heart. Wiley-Blackwell; 2009. Bicuspid aortic valve and aortic stenosis; p. 225-256.
5. Ward C. Clinical significance of the bicuspid aortic valve. Heart. 2000; 83:81–85. [PubMed: 10618341]
6. Schaefer BM, Lewin MB, Stout KK, Gill E, Prueitt A, Byers PH, Otto CM. The bicuspid aortic valve: An integrated phenotypic classification of leaflet morphology and aortic root shape. Heart. 2008; 94:1634–1638. [PubMed: 18308868]
7. Sievers HH, Schmidtke C. A classification system for the bicuspid aortic valve from 304 surgical specimens. J Thorac Cardiovasc Surg. 2007; 133:1226–1233. [PubMed: 17467434]
8. Fernandes SM, Khairy P, Sanders SP, Colan SD. Bicuspid aortic valve morphology and interventions in the young. J Am Coll Cardiol. 2007; 49:2211–2214. [PubMed: 17543642]
9. Girdauskas E, Borger MA, Secknus M-A, Girdauskas G, Kuntze T. Is aortopathy in bicuspid aortic valve disease a congenital defect or a result of abnormal hemodynamics? A critical reappraisal of a one-sided argument. Eur J Cardiothorac Surg. 2011; 39:809–814. [PubMed: 21342769]
10. Hope MD, Hope TA, Meadows AK, Ordovas KG, Urbania TH, Alley MT, Higgins CB. Bicuspid aortic valve: Four-dimensional mr evaluation of ascending aortic systolic flow patterns1. Radiology. 2010; 255:53–61. [PubMed: 20308444]
11. Lehoux S, Tedgui A. Cellular mechanics and gene expression in blood vessels. J Biomech. 2003; 36:631. [PubMed: 12694993]

12. Hope MD, Hope TA, Crook SES, Ordovas KG, Urbania TH, Alley MT, Higgins CB. 4d flow cmr in assessment of valve-related ascending aortic disease. JACC: Cardiovascular Imaging. 2011; 4:781–787. [PubMed: 21757170]

13. Barker AJ, Markl M. Editorial the role of hemodynamics in bicuspid aortic valve disease. Eur J Cardiothorac Surg. 2011; 39:805–806. [PubMed: 21339071]

14. Barker AJ, Lanning C, Shandas R. Quantification of hemodynamic wall shear stress in patients with bicuspid aortic valve using phase-contrast mri. Ann Biomed Eng. 2010; 38:788–800. [PubMed: 19953319]

15. Meierhofer C, Schneider EP, Lyko C, Hutter A, Martinoff S, Markl M, Hager A, Hess J, Stern H, Fratz S. Wall shear stress and flow patterns in the ascending aorta in patients with bicuspid aortic valves differ significantly from tricuspid aortic valves: A prospective study. Eur Heart J Cardiovasc Imaging. 2013; 14:797–804. doi: 10.1093/ehjci/jes273. Epub 2012 Dec 9. [PubMed: 23230276]

16. Barker AJ, Markl M, Bürk J, Lorenz R, Bock J, Bauer S, Schulz-Menger J, von Knobelsdorff-Brenkenhoff F. Bicuspid aortic valve is associated with altered wall shear stress in the ascending aortaclinical perspective. Circ Cardiovasc Imaging. 2012; 5:457–466. [PubMed: 22730420]

17. Bissell MM, Hess AT, Biasiolli L, Glaze SJ, Loudon M, Pitcher A, Davis A, Prendergast B, Markl M, Barker AJ, Neubauer S, Myerson SG. Aortic dilation in bicuspid aortic valve disease: Flow pattern is a major contributor and differs with valve fusion type. Circ Cardiovasc Imaging. 2013; 6:499–507. [PubMed: 23771987]

18. Kang J-W, Song HG, Yang DH, Baek S, Kim D-H, Song J-M, Kang D-H, Lim T-H, Song J-K. Association between bicuspid aortic valve phenotype and patterns of valvular dysfunction and bicuspid aortopathycomprehensive evaluation using mdct and echocardiography. JACC: Cardiovascular Imaging. 2013; 6:150–161. [PubMed: 23489528]

19. Markl M, Harloff A, Bley TA, Zaitsev M, Jung B, Weigang E, Langer M, Hennig J, Frydrychowicz A. Time-resolved 3d mr velocity mapping at 3t: Improved navigator-gated assessment of vascular anatomy and blood flow. J Mag Reson Imaging. 2007; 25:824–831.

20. Hiratzka LF, Bakris GL, Beckman JA, Bersin RM, Carr VF, Casey JDE, Eagle KA, Hermann LK, Isselbacher EM, Kazerooni EA, Kouchoukos NT, Lytle BW, Milewicz DM, Reich DL, Sen S, Shinn JA, Svensson LG, Williams DM. J Am Coll Cardiol. 2010; 55:e27–e129. 2010 accf/aha/aats/acr/asa/sca/scai/sir/sts/svm guidelines for the diagnosis and management of patients with thoracic aortic disease. [PubMed: 20359588]

21. Bonow RO, Carabello BA, Chatterjee K, de Leon JAC, Faxon DP, Freed MD, Gaasch WH, Lytle BW, Nishimura RA, O'Gara PT, O'Rourke RA, Otto CM, Shah PM, Shanewise JS, Nishimura RA, Carabello BA, Faxon DP, Freed MD, Lytle BW, O'Gara PT, O'Rourke RA, Shah PM. 2008 focused update incorporated into the acc/aha 2006 guidelines for the management of patients with valvular heart diseasea report of the american college of cardiology/american heart association task force on practice guidelines (writing committee to revise the 1998 guidelines for the management of patients with valvular heart disease) endorsed by the society of cardiovascular anesthesiologists, society for cardiovascular angiography and interventions, and society of thoracic surgeons. J Am Coll Cardiol. 2008; 52:e1–e142. [PubMed: 18848134]

22. Fazel SS, Mallidi HR, Lee RS, Sheehan MP, Liang D, Fleischman D, Herfkens R, Mitchell RS, Miller DC. The aortopathy of bicuspid aortic valve disease has distinctive patterns and usually involves the transverse aortic arch. J Thorac Cardiovasc Surg. 2008; 135:901–907. 907 e901-902. [PubMed: 18374778]

23. Bock, J.; Kreher, B.; Hennig, J.; Markl, M. Optimized pre-processing of time-resolved 2d and 3d phase contrast mri data. Proceedings of the 15th Annual Meeting of ISMRM, Berlin, Germany; 2007. p. 3138

24. Sigovan M, Hope MD, Dyverfeldt P, Saloner D. Comparison of four-dimensional flow parameters for quantification of flow eccentricity in the ascending aorta. J Mag Reson Imaging. 2011; 34:1226–1230.

25. Papathanasopoulou P, Zhao S, Köhler U, Robertson MB, Long Q, Hoskins P, Yun Xu X, Marshall I. Mri measurement of time-resolved wall shear stress vectors in a carotid bifurcation model, and comparison with cfd predictions. J Mag Reson Imaging. 2003; 17:153–162.

26. Stalder A, Russe M, Frydrychowicz A, Bock J, Hennig J, Markl M. Quantitative 2d and 3d phase contrast mri: Optimized analysis of blood flow and vessel wall parameters. Magn Reson Med. 2008; 60:1218–1231. [PubMed: 18956416]
27. Hope MD, Wrenn J, Sigovan M, Foster E, Tseng EE, Saloner D. Imaging biomarkers of aortic disease: Increased growth rates with eccentric systolic flow. J Am Coll Cardiol. 2012; 60:356–357. [PubMed: 22813616]
28. Verma S, Yanagawa B, Kalra S, Ruel M, Peterson MD, Yamashita MH, Fagan A, Currie ME, White CW, Wai Sang SL, Rosu C, Singh S, Mewhort H, Gupta N, Fedak PW. Knowledge, attitudes, and practice patterns in surgical management of bicuspid aortopathy: A survey of 100 cardiac surgeons. J Thorac Cardiovasc Surg. 2013; 146:1033–1040. e4. doi: 10.1016/j.jtcvs.2013.06.037. Epub 2013 Aug 26. [PubMed: 23988289]
29. Bürk J, Blanke P, Stankovic Z, Barker A, Russe M, Geiger J, Frydrychowicz A, Langer M, Markl M. Evaluation of 3d blood flow patterns and wall shear stress in the normal and dilated thoracic aorta using flow-sensitive 4d cmr. J Cardiovasc Magn Reson. 2012; 14:84. [PubMed: 23237187]
30. Hope TA, Markl M, Wigstrom L, Alley MT, Miller DC, Herfkens RJ. Comparison of flow patterns in ascending aortic aneurysms and volunteers using four-dimensional magnetic resonance velocity mapping. J Magn Reson Imaging. 2007; 26:1471–1479. [PubMed: 17968892]
31. Della Corte A, Bancone C, Conti CA, Votta E, Redaelli A, Del Viscovo L, Cotrufo M. Restricted cusp motion in right-left type of bicuspid aortic valves: A new risk marker for aortopathy. J Thorac Cardiovasc Surg. 2012; 144:360–369. 369 e361. [PubMed: 22050982]
32. Den Reijer PM, Sallee D III, Van Der Velden P, Zaaijer ER, Parks WJ, Ramamurthy S, Robbie TQ, Donati G, Lamphier C, Beekman RP. Hemodynamic predictors of aortic dilatation in bicuspid aortic valve by velocity-encoded cardiovascular magnetic resonance. J Cardiovasc Magn Reson. 2010; 12:4. doi: 10.1186/1532-429X-12-4. [PubMed: 20070904]

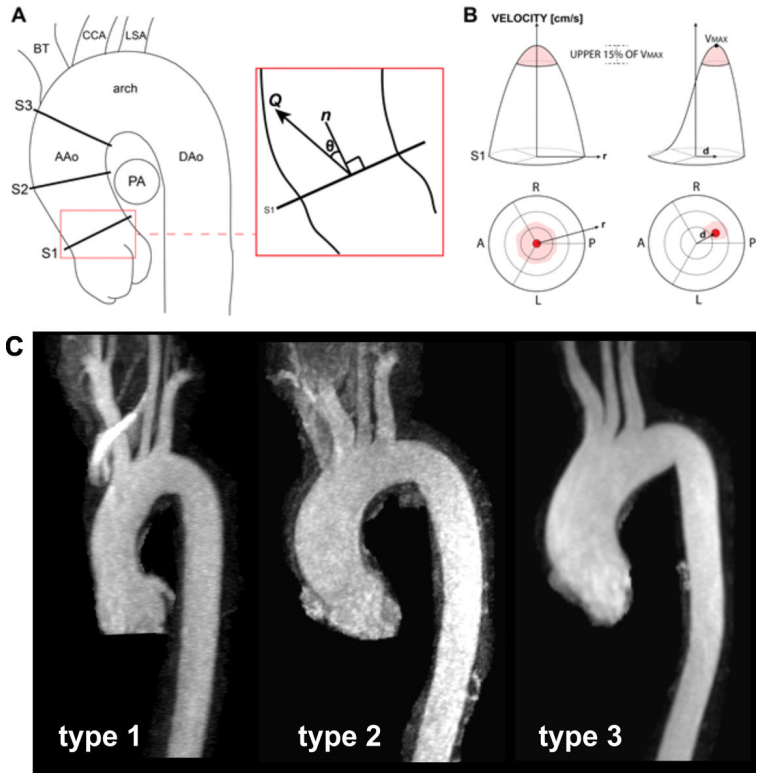

Figure 1.

A: Quantification of ascending aorta (AAo) hemodynamics in three analysis planes (S1, S2, S3) to compute the systolic flow angle, θ, between the net systolic flow, Q, and unit normal vector, n. **B:** The location of the top 15% of velocities at peak systole was mapped onto an aortic lumen chart. A symmetric flow profile is reflected by a central location of the maximum velocities (red shaded area) with the highest velocity (V_{Max}) at the center of the vessel. Flow profile asymmetry results in an off-center location of the top 15% of velocities. The flow displacement, d, calculated as the distance (in mm) from the vessel centroid to the velocity-weighted centroid. **C:** Example images illustrating the three different aortopathy types in our patient cohort. PA: pulmonary artery, DAo: descending aorta, CCA: common carotid artery, LSA: left subclavian artery, A: anterior, P: posterior, L: left, R: right, BT: brachiocephalic trunk.

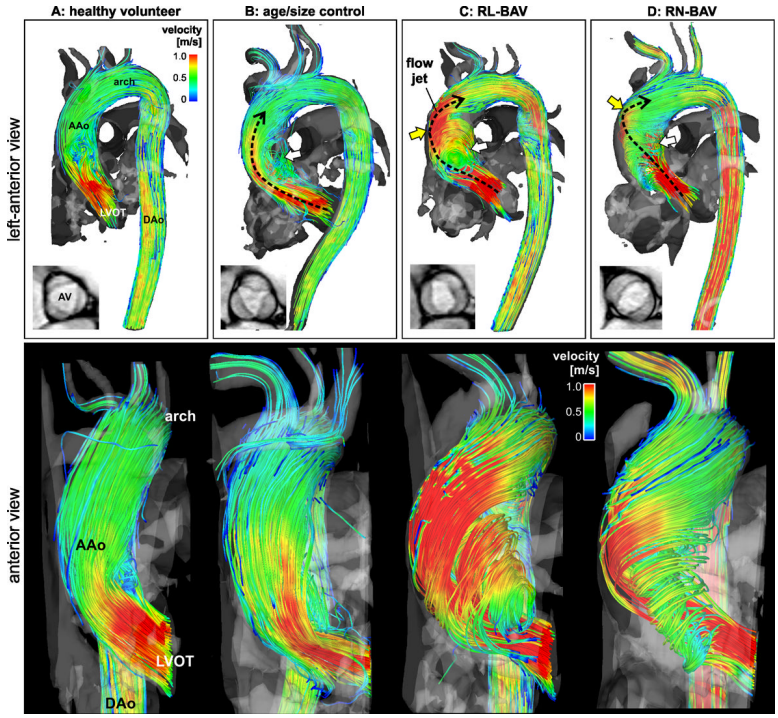

Figure 2.

Top row: 3D streamline visualization of peak systolic blood flow in patients with BAV (C,D) compared to an aorta size matched control subject (B) and a healthy volunteer (A). Note the presence of distinctly different 3D outflow flow jet patterns (black dashed arrows) in the ascending aorta (AAo) for patients B-C. **Bottom row:** 3D flow patterns in the left ventricular outflow tract (LVOT) and ascending aorta (AAo) distal to the aortic valve. Note the different systolic AV outflow flow jet patterns (red color indicating high velocities > 1m/s) and wall impingement zones which correspond to variable exertion of high wall shear forces between different valve groups (C,D) and aorta size matched controls (B) and healthy volunteers (A).

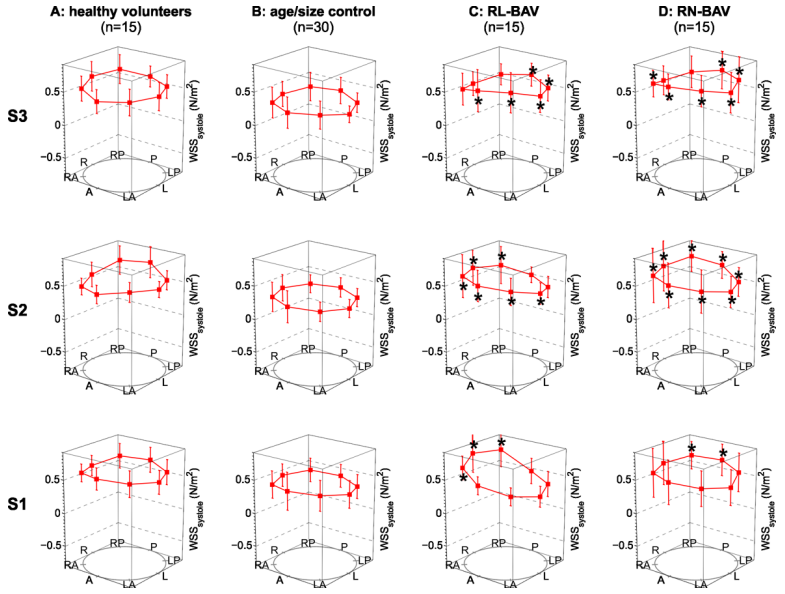

Figure 3.

Segmental systolic wall shear stress (WSS) measurements at the sinotubular junction (analysis plane S1), the mid ascending aorta (S2), and the distal ascending aorta (S3). The individual data points represent mean systolic WSS for patients with bicuspid aortic valves (C,D), aorta size matched controls (B), and healthy volunteers (A) across eight anatomical locations ("A" anterior, "LA" left anterior, "L" left, "LP" left posterior, "P" posterior, "RP" right posterior, "R" right, "RA" right anterior). Error bars represent the standard deviation of inter-individual WSS variation. * indicates statistically significant differences for RL-BAV and RN-BAV cohorts compared to aorta size matched controls ($p < 0.0125$ after Bonferroni correction).

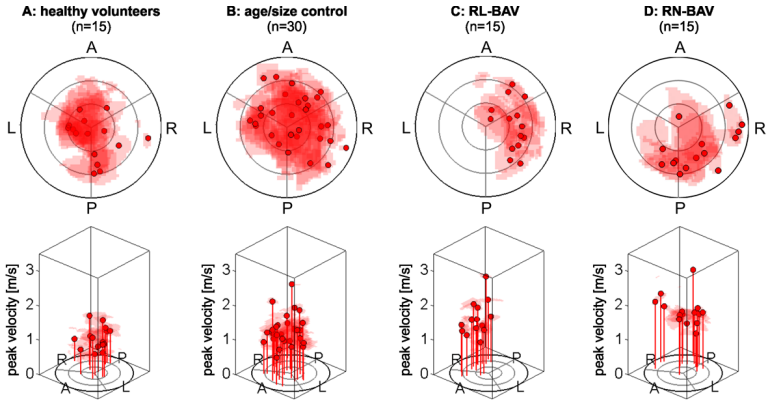

Figure 4.

Flow profile asymmetry maps schematically illustrating flow eccentricity using the locations of the upper 15% of systolic velocities for all participants within each cohort at the the sinotubular junction (analysis plane S1). RN-BAV patients showed outflow asymmetry towards the right posterior wall compared to RL-BAV, whose flow profile was directed towards the right-wall. (“A” anterior, “L” left, “P” posterior, “R” right). Note that each subject’s profile map was normalized to their sinotubular junction diameter.

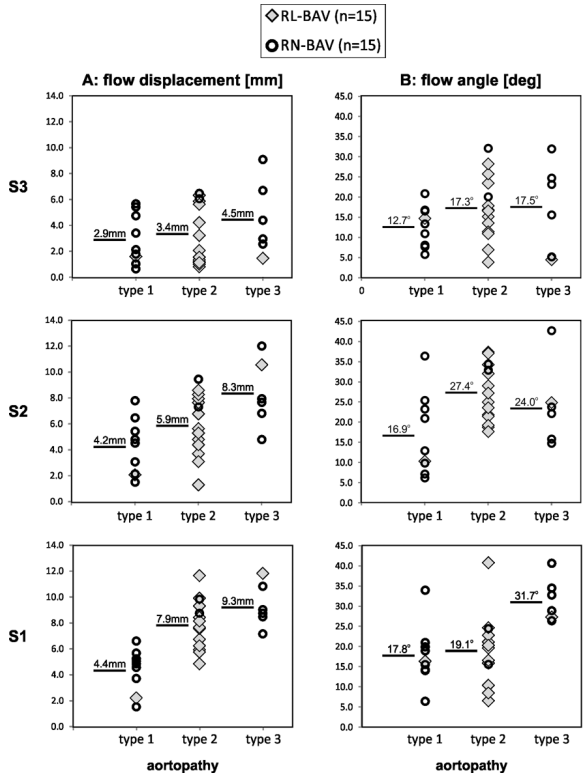

Figure 5.

Distribution of flow angle and outflow asymmetry (flow displacement *d*) for all BAV patients as a function of aortopathy phenotype. The numbers represent mean flow angle or displacement for each aortopathy type 1, 2 or 3. Note that statistical comparisons were not performed due to the small number of subjects with type 3 and type 1.

Table 1

Descriptive statistics of patient demographics, aortic dimensions, and hemodynamic parameters at the three analysis planes S1 (sinotubular junction), S2 (MAA), and S3 (distal ascending aorta). MAA: mid ascending aortic, SOV: sinus of valsalva. All continuous data are presented as mean ± standard deviation (median, interquartile range).

		Tricuspid valve		Bicuspid valve	
		healthy volunteers	**aorta size controls**	**RL-BAV**	**RN-BAV**
n (female)		15 (5)	30 (5)	15 (3)	15 (4)
Age		32.6 ± 7.6 (31.0, 7.5)	59.2 ± 12.5 (58.5, 16.2)	47.5 ± 11.5* (45.3, 17.5)	44.7 ± 8.0* (45.0, 10.1)
MAA Diameter [mm]		24.9 ± 3.0 (25.0, 4.9)	41.0 ± 4.4 (42.0, 5.8)	39.9 ± 4.4 (40.0, 3.5)	39.6 ± 7.2 (38.0, 1.0)
SOV Diameter [mm]		-	42.3 ± 4.6 (42.0, 5.0)	40.5 ± 2.7 (40.0, 3.5)	43.9 ± 4.9 (43.0, 3.0)
Aortopathy	**Type 0**	15 (100%)	-	-	-
	Type 1	0	9 (30%)	1 (7%)	8 (53%)
	Type 2	0	13 (43%)	13 (87%)	2 (13%)
	Type 3	0	8 (27%)	1 (7%)	5 (34%)
systolic WSS [N/m^2]	**S1**	0.60 ± 0.15* (0.61, 0.15)	0.41 ± 0.16 (0.38, 0.24)	0.55 ± 0.16* (0.50, 0.18)	0.58 ± 0.18* (0.58, 0.30)
	S2	0.56 ± 0.14* (0.63, 0.22)	0.30 ± 0.14 (0.28, 0.18)	0.56 ± 0.18* (0.53, 0.19)	0.61 ± 0.21* (0.57, 0.30)
	S3	0.55 ± 0.16 # (0.52, 0.23)	0.32 ± 0.16 (0.31, 0.22)	0.56 ± 0.19 # (0.59, 0.25)	0.62 ± 0.21 # (0.56, 0.36)
Valve flow angle [°]	**S1**	6.3 ± 3.5 # (4.5, 5.5)	18.0 ± 10.8 (16.1, 12.7)	19.4 ± 8.6 (19.9, 6.4)	23.2 ± 9.6 (21.0, 15.3)
	S2	8.4 ± 4.8 # (7.4, 6.5)	19.6 ± 12.4 (17.9, 16.6)	25.3 ± 7.7 (24.9, 10.2)	21.9 ± 11.1 (22.1, 15.3)
	S3	13.1 ± 8.1 (12.7, 12.2)	11.0 ± 7.0 (9.1, 9.2)	15.1 ± 7.1 (15.1, 6.2)	16.8 ± 8.7 (16.5, 12.5)
flow displacement *d*	**S1**	1.8 ± 1.5 # (1.4, 0.7)	3.9 ± 2.3 (3.2, 4.0)	7.6 ± 2.6 # (7.6, 3.1)	6.7 ± 2.6 # (6.6, 3.8)
[mm]	**S2**	1.2 ± 0.5* (1.2, 0.7)	4.3 ± 2.7 (3.9, 4.0)	5.7 ± 2.6 (5.3, 3.8)	6.1 ± 2.8 (6.5, 3.1)
	S3	1.3 ± 0.5 # (1.3, 0.7)	2.5 ± 2.4 (1.6, 0.6)	2.8 ± 2.0 (1.6, 3.0)	4.2 ± 2.4# (4.4, 3.5)

*, # denotes significant differences compared with aorta size matched controls ($p<0.0125$ after Bonferroni correction);

* = independent-sample t-test,

= Mann-Whitney test